

Quantum phase transition in transverse-field Ising model on Sierpiński gasket lattice

Tymoteusz Braciszewski,* Oliwier Urbański,† and Piotr Tomczak‡

Faculty of Physics and Astronomy, Adam Mickiewicz University,

Uniwersytetu Poznańskiego 2, 61-614 Poznań, Poland

(Dated: February 4, 2026)

Abstract

We study quantum phase transition in the transverse-field Ising model on the Sierpiński gasket. By applying finite-size scaling and numerical renormalization group methods, we determine the critical coupling and the exponents that describe this transition. We first checked our finite-size scaling and the renormalization methods on the exactly solvable one-dimensional chain, where we recovered proper values of critical couplings and exponents. Then, we applied the method to the Sierpiński gasket with 11 and 15 spins. We found a quantum critical point at $\lambda_c \approx 2.72$ to 2.93 , with critical exponents $z \approx 0.84$, $\nu \approx 1.12$, $\beta \approx 0.30$, and $\gamma \approx 2.54$. The lower dynamical exponent z indicates that quantum fluctuations slow down due to fractal geometry, yielding an effective critical dimension of about 2.43. The numerical renormalization group method yielded similar results $\lambda_c = 2.765$, $\beta = 0.306$, supporting our findings. These exponents differ from those in both the one-dimensional and mean-field cases.

I. INTRODUCTION

Quantum phase transitions in spin systems on fractal lattices with non-integer Hausdorff dimensions offer a unique opportunity to explore the intricate relationships between geometry and the universality of critical behavior [1, 2, 4]. The transverse-field Ising model (TFIM) defined on the Sierpiński gasket, a fractal lattice with a Hausdorff dimension of $d_H = \ln 3 / \ln 2 \approx 1.585$, is particularly insightful in this context. Unlike the exactly solvable one-dimensional chain, where the dynamical exponent is strictly $z = 1$, the fractal geometry of the gasket also leads to a change of z . This alteration also impacts the remaining critical exponents [5–7].

This paper demonstrates, using two complementary methods, finite-size scaling (FSS) and the numerical renormalization group (NRG), how to obtain reliable information about critical couplings and exponents of the TFIM defined on the Sierpiński gasket lattice by studying the properties of small systems away from the thermodynamic limit.

The paper is organized into four sections. In Sec. II, we apply FSS analysis to the

* e-mail: tymbra@st.amu.edu.pl

† e-mail: oliurb4@st.amu.edu.pl

‡ e-mail: ptomczak@amu.edu.pl

one-dimensional TFIM,

$$H = -J \sum_{i=1}^N \sigma_i^x \sigma_{i+1}^x - h \sum_{i=1}^N \sigma_i^z, \quad (1a)$$

or

$$H/J = - \sum_{i=1}^N \sigma_i^x \sigma_{i+1}^x - \lambda \sum_{i=1}^N \sigma_i^z, \quad (1b)$$

the first sum runs over all nearest-neighbor pairs on a given lattice, and $\lambda = h/J$ is the dimensionless transverse field strength. For the FSS we use small systems with up to $N = 18$ spins with periodic boundary conditions. This approach serves as a strong benchmark for our numerical method. Even with these small systems, we recover the exact critical point $\lambda_c = 1$ and the exponents $z = 1$, $\nu = 1$, $\beta = 0.125$, and $\gamma = 1.75$ with relatively small errors, which shows that this method can be used even outside the large-size, asymptotic regime. In the Sec. III, we use the same FSS technique to study the critical behaviour of the TFIM on the Sierpiński gasket. Using systems with up to $N = 15$ spins, we find the quantum critical point $\lambda_c \approx 2.72 - 2.93$ and the critical exponents $z \approx 0.84$, $\nu \approx 1.12$, $\beta \approx 0.30$, and $\gamma \approx 2.54$.

In the Sec. IV, we revisit the earlier version of the RG method for quantum systems [3] and reproduce some of the original results for the Ising spin chain in a transverse field. Finally, in Sec. V, we apply the same method to the TFIM on the Sierpiński gasket lattice and find results that are qualitatively similar to those from the FSS approach. The article ends with a short summary.

II. FINITE-SIZE SCALING BENCHMARK ON THE ONE-DIMENSIONAL TFIM

We select the one-dimensional transverse-field Ising model, which has an exact solution, to evaluate the FSS procedure under challenging conditions, i.e., for small system sizes of $N = 6, 10, 14, 16, 18$ and exclude larger systems with periodic boundary conditions. To perform finite-size scaling, the lowest energies $E_0(N, \lambda)$ and $E_1(N, \lambda)$ and their corresponding eigenstates $|\psi_0(N, \lambda)\rangle$ and $|\psi_1(N, \lambda)\rangle$ are obtained numerically using the exact diagonalization (ED) procedure, specifically we used the Lanczos algorithm.

Subsequently we examine FSS of the

- Binder cumulant $U_N = \frac{3}{2} \left(1 - \frac{\langle m^4 \rangle}{3 \langle m^2 \rangle^2} \right)$,

- magnetization $m(N, \lambda) = \frac{1}{N} \langle \psi_0(N, \lambda) | \text{abs}(\sum_{i=1}^N \sigma_i^z) | \psi_0(N, \lambda) \rangle$,
- gap in the energy spectrum $\Delta(N, \lambda) = E_1(N, \lambda) - E_0(N, \lambda)$,
- and magnetic susceptibility $\chi = \frac{\partial m}{\partial \lambda} \Big|_{\lambda=\lambda_c}$.

The standard finite-size scaling ansatz for quantum critical points states that the data for different system sizes fall onto a single curve for appropriately scaled arguments and scaled function values near the critical point. We call that curve a scaling function. Putting $\tilde{\lambda} = (\lambda - \lambda_c)/\lambda_c$ we have

$$U_N(\lambda, N) = \mathcal{B}(\tilde{\lambda} N^{1/\nu}), \quad (2)$$

Here, \mathcal{B} is the scaling function for the Binder cumulant. Similarly,

$$\Delta(\lambda, N) N^z = \mathcal{G}(\tilde{\lambda} N^{1/\nu}), \quad (3)$$

$$m(\lambda, N) N^{\beta/\nu} = \mathcal{M}(\tilde{\lambda} N^{1/\nu}), \quad (4)$$

and

$$\chi(\lambda, N) N^{-\gamma/\nu} = \mathcal{X}(\tilde{\lambda} N^{1/\nu}), \quad (5)$$

where \mathcal{G} , \mathcal{M} , and \mathcal{X} are the appropriate scaling functions. Let us examine FSS of Binder

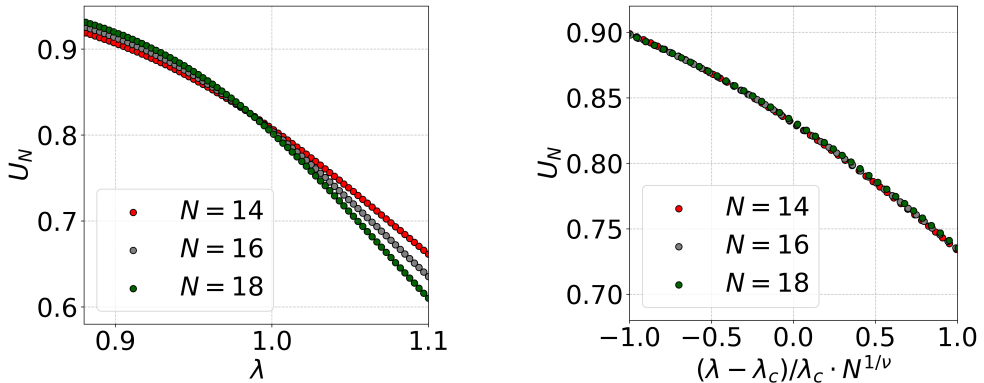


FIG. 1. The Binder cumulant before (left) and after rescaling (right). As expected from the finite size scaling ansatz, Eq. (2), the data for system sizes $N=14, 16, 18$ fall onto a single curve for $\lambda_c = 0.9835, \nu = 1.0044$ (right).

cumulant in detail. Using data from ED as input, we treat λ_c and ν as free fitting parameters

and perform a global nonlinear least-squares fit of Eq. (2) to all $\Delta(\lambda, N)$ in the window $|\tilde{\lambda}N^{\frac{1}{\nu}}| < 2$. Even with only two system sizes $N=18$ and 16 , the fit converges and yields: $\lambda_c = 0.9857$, $\nu = 1.0050$, see first row and first column of Table I. The results for scaling systems of other sizes are shown in the first column of this table, while the Binder cumulant before and after scaling is shown in Fig. 1.

The remaining columns of Table I show the critical points and exponents from the collapse of magnetization, gap, and susceptibility. FSS slightly underestimates λ_c and overestimates ν when only the exponents related to correlation length divergence (ν) are used for scaling. This tendency reverses when the exponents (β and γ) related to the magnetic field (λ) are used together.

This behavior is clearly visible in the scaling collapse of the order parameter m , see Fig. 2. Using the system sizes ($N = 14 - 18$), the optimal collapse yields $\lambda_c \approx 1.0051$, $\beta \approx 0.1253$, and $\nu \approx 0.9157$. The value of β is already very close to the exact Ising exponent $\beta = 1/8$, whereas the estimate of ν is noticeably smaller than the expected value $\nu = 1$. This discrepancy is attributed to finite-size corrections, which are known to strongly affect multi-parameter scaling collapses and can lead to a systematic overestimation of λ_c and an effective reduction of ν . The consistency of the drift in λ_c observed across both Binder cumulant and magnetization collapses further supports this interpretation.

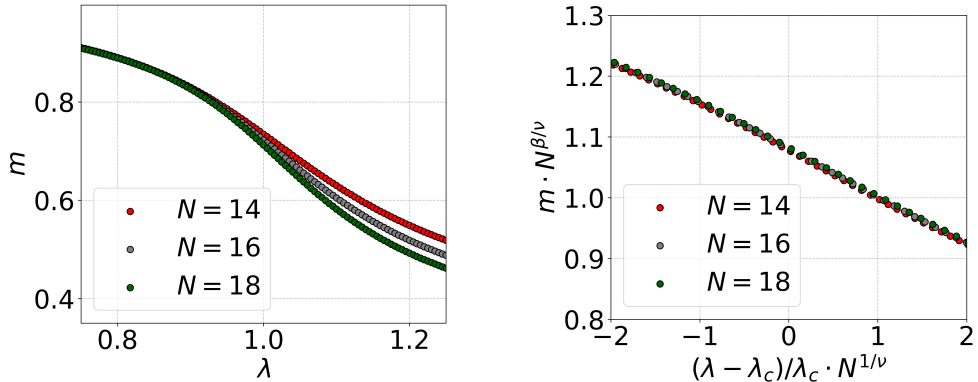


FIG. 2. The magnetization before (left) and after rescaling (right) according to the Eq. 4. The values of m calculated for system sizes $N = 14, 16, 18$ fall onto a single curve for $\lambda_c = 1.0051$, $\beta = 0.1253$, and $\nu = 0.9157$ (right). This collapse was obtained with fitted parameters differing by 0.3% from the exact value of β and 8% from the exact value of ν - it shows the robustness of the FSS procedure even for very small systems.

Let us briefly discuss the gap scaling and the method used to determine the exponent z . The fourth column of the Table presents the values of ν found by assuming $z = 1$. Taking for the FSS of gap $\Delta(\lambda, N)$ the values of ν obtained from the scaling of m yield a slightly lower value of $z = 0.9648$. This indicates a minor deviation from criticality, attributable to the increased sensitivity of m to subleading corrections in small systems. Figure 3 presents the scaled data collapse. When ΔN^z is plotted against the scaling variable $\tilde{\lambda} N^{1/\nu}$, the curves for all three system sizes align on a single universal curve with minimal visible scatter.

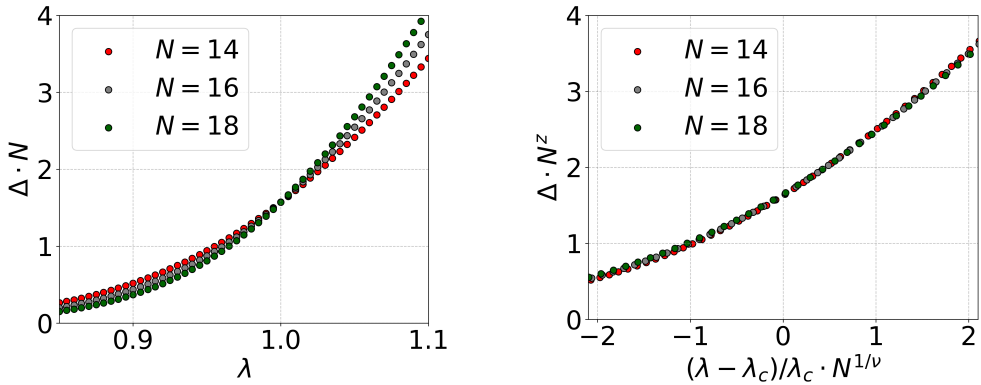


FIG. 3. The gap between ground state and first excited state before (left) and after rescaling (right). The values of the gap calculated for system sizes $N = 14, 16, 18$ fall onto a single curve for $\lambda_c = 0.9998$ and $\nu = 1.0123$ (right). To perform this scaling, $z = 1$ was assumed. Taking the value of ν from the scaling, for example of m and fixing it, yields a slightly lower value of z ; see the text.

The results of the benchmark confirm that our FSS approach, including the choice of fitting window and numerical differentiation of m , is accurate and stable enough to be confidently applied to the more challenging fractal geometry of the Sierpiński gasket. In this case, exact results are unavailable, and system sizes must remain modest.

III. SIERPIŃSKI GASKET - FSS ANALYSIS

Having validated our FSS approach on the exactly solvable one-dimensional chain, we now apply the same methodology to the transverse-field Ising model on the Sierpiński gasket lattice. Like the periodic chain, the gasket has also periodic boundary conditions, i.e., with corner sites not playing a special geometric role, see Fig. 4.

We studied gasket systems of sizes $N = 11, 15$ spins, see Fig. 4. For each system size and

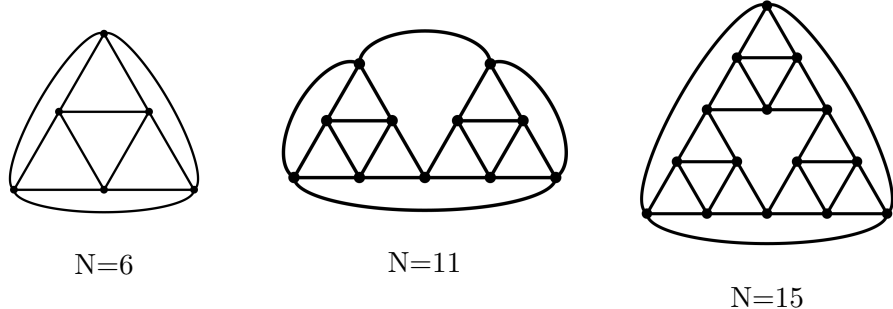


FIG. 4. Sierpiński gasket lattices with periodic boundary conditions.

field strength λ , we obtained the ground state $|\psi_0(N, \lambda)\rangle$ and first excited state $|\psi_1(N, \lambda)\rangle$ through exact diagonalization using the Lanczos algorithm. From these eigenstates, we computed the same set of observables as in Section II: the Binder cumulant U_N , magnetization m , energy gap Δ , and magnetic susceptibility χ .

Exact diagonalization procedure was enhanced by exploiting symmetries of the system. Two operators realizing symmetry transformations were used – a rotation R by 120° of the entire lattice and a global spin flip F , with respect to x -axis. Since both of these operators commute with the Hamiltonian (and with each other), their eigenstates can be used to block-diagonalize the Hamiltonian. In other words, energy eigenstates of the system can be chosen to belong to specific eigenspaces of both R and F . For $J, h > 0$ mean energy is minimized when quantum amplitudes of all spin configurations have the same phase. Thus, on the basis of variational principle, ground state can be chosen to have all amplitudes positive real, so it necessarily lives in the eigenspace with $R = 1$ and $F = 1$. Dimensionality of this subspace is 5472 for the 15-spin gasket, which is roughly equal to $2^{15}/6$.

The finite-size scaling analysis follows the same procedure outlined in Section II, with the scaling ansatz given by Eqs. (2)-(5). We performed global nonlinear least-squares fits treating λ_c and the relevant critical exponents as free parameters. The fitting window was restricted to $|\tilde{\lambda}N^{1/\nu}| < 1.0$ to minimize contributions from subleading corrections, which are expected to be more pronounced on the fractal geometry than on the regular chain.

Figure 5 shows the Binder cumulant before and after scaling for the two largest system sizes ($N = 15, 11$). The collapse yields $\lambda_c = 2.7239(18)$ and $\nu = 1.1296(17)$, demonstrating data collapse despite the modest system sizes. The critical coupling is significantly larger than unity, reflecting the enhanced role of quantum fluctuations on the fractal geometry compared to the one-dimensional chain.

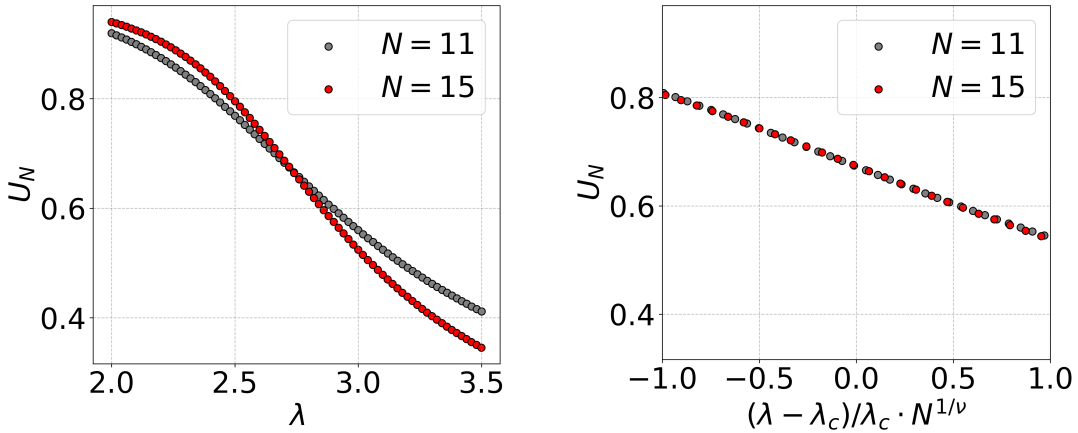


FIG. 5. The Binder cumulant for the Sierpiński gasket before (left) and after rescaling (right). The data for system sizes $N = 11, 15$ collapse onto a single curve for $\lambda_c = 2.7239$ and $\nu = 1.1296$.

The magnetization scaling, shown in Fig. 6, yields $\lambda_c = 2.9304(57)$, $\beta = 0.3002(45)$, and $\nu = 1.0962(64)$ for the two-size collapse. The value of β is notably larger than the one-dimensional result ($\beta = 1/8$), indicating a fundamental change in the order parameter behavior due to the fractal geometry.

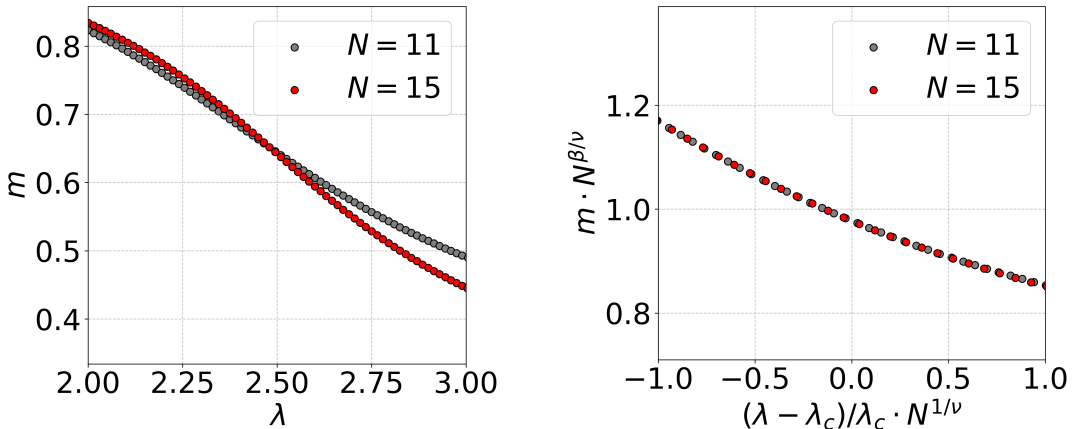


FIG. 6. The magnetization for the Sierpiński gasket before (left) and after rescaling (right). The collapse for $N = 11, 15$ yields $\lambda_c = 2.9304$, $\beta = 0.3002$, and $\nu = 1.0962$.

Figure 7 presents the scaling collapse of the energy gap. Using the value of ν from the Binder cumulant analysis and treating z as a free parameter, we obtain $z = 0.8400(27)$ for the $N = 15, 11$ collapse. This represents a substantial decrease compared to the one-

dimensional result $z = 1$, confirming that the fractal geometry significantly enhances the effective dimensionality of the quantum critical point. The dynamical exponent reflects the slowing down of quantum fluctuations due to the increased connectivity and bottlenecks inherent in the gasket structure.

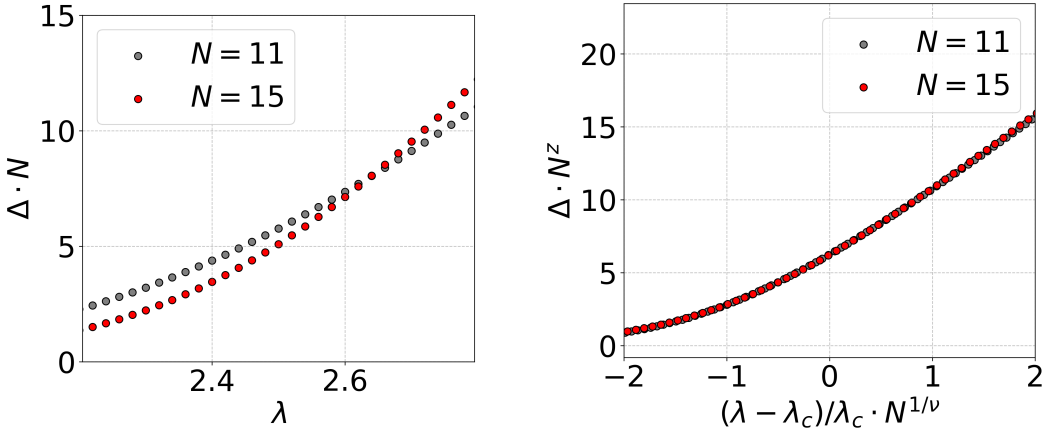


FIG. 7. The energy gap for the Sierpiński gasket before (left) and after rescaling (right). The scaling for $N = 11, 15$ with $\lambda_c = 2.9153$ and $\nu = 1.4219$ yields $z = 0.8400$.

Finally, the susceptibility collapse gives $\lambda_c = 2.7801(58)$, $\gamma = 2.5383(74)$, and $\nu = 1.5544(89)$. The large value of γ indicates strong critical fluctuations near the transition, again consistent with the enhanced effective dimensionality of the fractal lattice.

Table II summarizes all FSS results for both the two-size ($N = 15, 11$) collapses. The spread in λ_c estimates from different observables ranges from approximately 2.70 to 2.93, with the Binder cumulant providing the most stable estimate due to its reduced sensitivity to boundary effects. The correlation length exponent $\nu \approx 1.1$ is remarkably consistent across different observables (excluding the gap analysis where it is entangled with z), suggesting that this value is robust despite finite-size effects.

IV. NUMERICAL RENORMALIZATION GROUP METHOD APPLIED TO TFIM ON A 1D CHAIN.

To validate our FSS results we used another method common in studies of critical phenomena – Numerical Renormalization Group (NRG). In this method the spins are blocked

into non-interacting subsystems (blocks). Within each block, the ground state and first excited state are found by numerical diagonalization. In the next step of the renormalization procedure, each block is replaced by a single spin in a self-similar manner, and the hamiltonian for the new system is obtained by rescaling the couplings.

This method has been successfully applied to our model example of 1D-TFIM by Jullien et al. [3]. We reobtained their results for 1D-TFIM and then modified the method to calculate the critical properties of TFIM on the Sierpiński gasket. After grouping spins into block of size N spins we diagonalize Hamiltonian, Eq. (1), within one block. We label the ground and first excited states as $|\tilde{0}\rangle$, $|\tilde{1}\rangle$ respectively, with their energies labeled E_0 , E_1 . The diagonalized Hamiltonian has the form

$$H = \sum_{j=1}^N E_j |j\rangle\langle j| = E_0 |\tilde{0}\rangle\langle\tilde{0}| + E_1 |\tilde{1}\rangle\langle\tilde{1}| + \dots, \quad (6)$$

which can be truncated to the two lowest energy states as follows

$$\begin{aligned} \tilde{H} &= E_0 |\tilde{0}\rangle\langle\tilde{0}| + E_1 |\tilde{1}\rangle\langle\tilde{1}| \\ &= -\frac{E_1 - E_0}{2} \tilde{\sigma}^z + \frac{E_0 + E_1}{2} \tilde{I}, \end{aligned} \quad (7)$$

where $\tilde{\sigma}^z$, \tilde{I} are the "renormalized" spin- z Pauli matrix and the identity in the two-dimensional, single-spin Hilbert space. We recognize this Hamiltonian describes a single spin coupled to a field, with the renormalized coupling

$$\tilde{h} = \frac{E_1 - E_0}{2}. \quad (8)$$

To complete the renormalization procedure we include the coupling between adjacent blocks, $-J\sigma_i^x\sigma_j^x$. To this end we calculate the elements of σ_j^x between the $|\tilde{0}\rangle$, $|\tilde{1}\rangle$ states. The parity of energy eigenstates turns out to be crucial – since the terms in hamiltonian (1) cannot change the parity of an N -spin basis state, and the operator σ_j^x flips a single spin, it becomes apparent that

$$\langle\tilde{0}|\sigma_j^x|\tilde{0}\rangle = \langle\tilde{1}|\sigma_j^x|\tilde{1}\rangle = 0. \quad (9)$$

Since the block hamiltonian is a real matrix, its basis vectors can be chosen to be real. σ_j^x is real symmetric, so we can define

$$\xi_j = \langle\tilde{0}|\sigma_j^x|\tilde{1}\rangle = \langle\tilde{1}|\sigma_j^x|\tilde{0}\rangle. \quad (10)$$

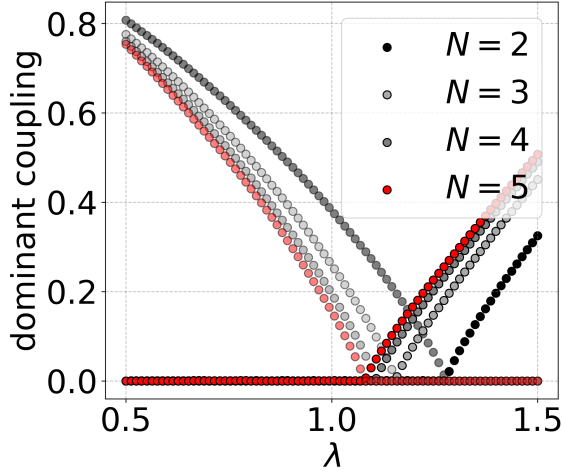


FIG. 8. Renormalized couplings J (to the left of the critical points, slightly transparent) and h (to the right). We see that below critical coupling, spin-spin ordering dominates while magnetic field coupling is renormalized to 0. Above the critical point the roles are reversed and the prevailing coupling is h , with $J \rightarrow 0$ with each step of the renormalization procedure.

The renormalized interaction term is thus of the form

$$-(J\xi_i\xi_j)\tilde{\sigma}_i^x\tilde{\sigma}_j^x = -\tilde{J}\tilde{\sigma}_i^x\tilde{\sigma}_j^x. \quad (11)$$

Having calculated the renormalized couplings we can write down the renormalization group equations. For the 1D-TFIM, the coupling between blocks is a single bond between the first and the last spin in the N -sized block. Due to symmetry the associated scaling factors ξ_1, ξ_N must be equal and thus we can write the hamiltonian at the n -th step of the renormalization procedure as

$$H_n = -J_n \sum \tilde{\sigma}_i^x \tilde{\sigma}_{i+1}^x - h_n \sum \tilde{\sigma}_i^z + C_n \tilde{I}. \quad (12)$$

With the couplings given by the following recurrence relations

$$\begin{aligned} h_{n+1} &= \frac{E_{1,n} - E_{0,n}}{2}, \\ J_{n+1} &= \xi_{N,n}^2 J_n, \\ C_{n+1} &= N C_n + \frac{E_{0,n} + E_{1,n}}{2}. \end{aligned} \quad (13)$$

The results of coupling renormalization can be seen in Fig. 8. To calculate the magnetization

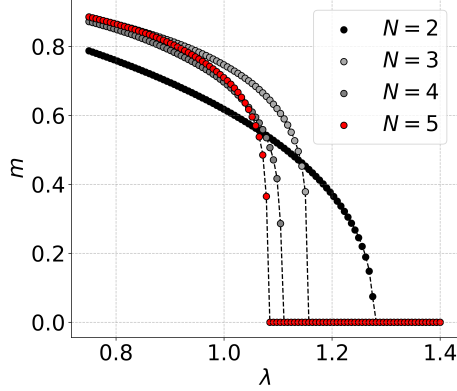


FIG. 9. Renormalized magnetization for the 1D chain.

it needs to be noted that the most representative member of the block is the spin in the middle. We can then calculate the renormalization of magnetization in a similar manner to the scaling factor of σ^x in Eq. (10) as follows

$$\begin{aligned}
 m_{n+1} &= \langle \tilde{\sigma}_{\text{mid}}^x \rangle_{n+1} \\
 &= \xi_{\text{mid}} \langle \tilde{\sigma}_{\text{mid}}^x \rangle_n \\
 &= \xi_{\text{mid}} m_n.
 \end{aligned} \tag{14}$$

with ξ_{mid} equal to $\xi_{N/2}$ for N even, $\xi_{(N+1)/2}$ for N odd. The plots of renormalized magnetization for blocks of sizes $N = 2, 3, 4, 5$ can be seen in Fig. 9.

V. NUMERICAL RENORMALIZATION GROUP APPLIED TO THE SIERPIŃSKI GASKET

In order to apply the NRG method to TFIM on the Sierpinski gasket we devised a suitable blocking procedure. We label the gasket at each step of construction as T_1, T_2, \dots such that T_1 is a triangle, T_2 is three triangles and so on. A block B_k is now defined as two T_k gaskets with one mutual corner, and one other (inequivalent) corner removed from each. Since T_k is made of $(3^k + 3)/2$ points, then B_k contains $L = 3^k$ spins – we shall investigate only $N = 3$ and $N = 9$ spin blocks which can be efficiently diagonalized.

Since each renormalized bond is now composed of two original inter-block bonds, renormalization group equations need to be modified. Each new bond is composed of interactions between the outermost spin of the block with two of the inner spins (as can be seen in Fig.

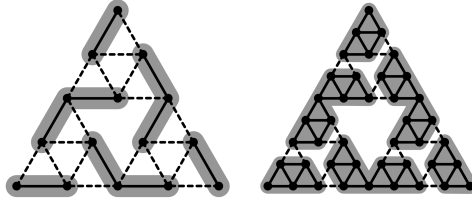


FIG. 10. Blocking procedure for $N = 3$ and $N = 9$ spin blocks.

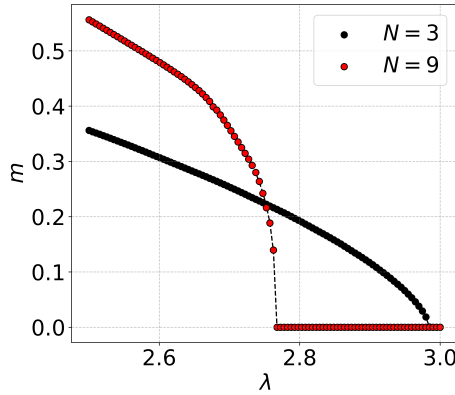


FIG. 11. Renormalized magnetization for the Sierpiński gasket.

10). The renormalization group equations are thus

$$\begin{aligned}
 h_{n+1} &= \frac{E_{1,n} - E_{0,n}}{2}, \\
 J_{n+1} &= \xi_a(\xi_b + \xi_c)J_n, \\
 C_{n+1} &= N C_n + \frac{E_{0,n} + E_{1,n}}{2}.
 \end{aligned} \tag{15}$$

The magnetization, resulting from above equations, is plotted in Fig. 11.

The critical coupling strength and β exponent can be found by fitting a power law $m \propto (\lambda - \lambda_c)^\beta$ to the magnetization values in the vicinity of λ_c . Table III collects the fitted parameters for both 1D chain and the Sierpiński gasket. As can be seen for the 1D chain, the results get closer to the exact values of $\lambda_c = 1$ and $\beta = 0.125$ the bigger L is, which is expected. For $N = 5$ blocking of the 1D chain the ratio of inter-block bonds to intra-block ones is 0.5, while for the $N = 9$ blocks on the gasket, the ratio is $9/14 \approx 0.64$, which is comparable, so the results for the gasket can be trusted (the method works better when this ratio is as small as possible).

VI. SUMMARY

This paper investigates quantum phase transitions in the transverse-field Ising model on the Sierpiński gasket. We employed two complementary numerical methods — finite-size scaling and the numerical renormalization group — to determine critical couplings and critical exponents at this phase transition.

We first validated our FSS approach by applying it to the exactly solvable one-dimensional TFIM chain with periodic boundary conditions. Using small systems with $N = 6, 10, 14, 16, 18$ spins, we recovered the exact critical point $\lambda_c = 1$ and the critical exponents $z = 1$, $\nu = 1$, $\beta = 0.125$, and $\gamma = 1.75$ with small statistical errors. This benchmark shows that reliable critical exponent extraction is possible even for modest system sizes outside the large-size regime.

Applying the same FSS methodology to the Sierpiński gasket with systems of $N = 11, 15$ spins and periodic boundary conditions, we obtained critical parameters from scaling collapses of the Binder cumulant, magnetization, energy gap, and magnetic susceptibility. Our analysis yields a critical point in the range $\lambda_c \approx 2.72\text{--}2.93$, depending on the observable. The Binder cumulant provides the most stable estimate of $\lambda_c = 2.7239(18)$ because of its reduced sensitivity to boundary effects. The critical exponents are $\nu \approx 1.1$, $\beta \approx 0.30$, $z \approx 0.84$, and $\gamma \approx 2.54$.

The dynamical exponent $z \approx 0.8400$ is a substantial decrease compared to the one-dimensional result $z = 1$. This reflects the slowing of quantum fluctuations caused by the fractal geometry. The effective critical dimensionality is $d_{\text{eff}} = d_H + z \approx 1.59 + 0.84 \approx 2.43$, which exceeds both the Hausdorff dimension and the geometric embedding dimension. This explains the departure from mean-field exponents and shows how fractal geometry alters quantum critical universality. The order parameter exponent $\beta \approx 0.30$ is larger than the one-dimensional Ising value $\beta = 1/8$, indicating a fundamental change in critical behavior.

To validate our FSS results, we applied the numerical renormalization group method, following the approach of Jullien et al. [3] for the one-dimensional chain and extending it to the Sierpiński gasket. We successfully reproduced the original NRG results for the 1D-TFIM, obtaining critical parameters that converge to exact values as the block size N increases. For the gasket, we implemented a blocking procedure with $L = 3$ and $N = 9$ spin blocks and obtained $\lambda_c = 2.765$ and $\beta = 0.306$ for the larger block size, in good qualitative agreement

with the FSS analysis.

Our FSS results are not consistent with Monte Carlo simulations [6], which reported slightly different values for λ_c (1.865) and different values of critical exponents. The agreement between our small-system exact diagonalization and independent NRG analysis validates both methods and confirms the reliability of critical exponent extraction in the regime of fractal lattices with limited system sizes. The consistency between FSS and NRG methods provides strong evidence that the critical behavior of TFIM on the Sierpiński gasket is governed by non-trivial critical exponents that differ from both the one-dimensional chain and mean-field predictions. The enhanced effective dimensionality, $d_{\text{eff}} \approx 2.43$, indicates that fractal geometry plays a crucial role in quantum critical phenomena: the non-integer Hausdorff dimension and complex geometry lead to emergent critical behavior that simple dimensional arguments cannot capture.

- [1] Y. Gefen, A. Aharony, B. B. Mandelbrot, and S. Kirkpatrick, Phys. Rev. Lett. **47**, 1771 (1981).
- [2] Y. Gefen, A. Aharony, and B. B. Mandelbrot, J. Phys. A **17**, 1277 (1984).
- [3] R. Jullien, P. Pfeuty, J.N. Fields, and S. Doniach, Phys. Rev. B **18** 3568 (1978).
- [4] P. Tomczak, W. Jeżewski, Physica A **209**, 275 (1994).
- [5] I. A. Kovács and F. Iglói, Phys. Rev. B **82**, 054437 (2010).
- [6] Hangmo Yi, Phys. Rev. E **91**, 012118 (2015).
- [7] R. Krcmar, J. Genzor, Y. Lee, H. Čenčariková, T. Nishino, and A. Gendiar, Phys. Rev. E **98**, 062114 (2018).

TABLE I. Critical points and critical exponents obtained for 1D TFIM from FSS of small systems. The quantities used for FSS are in the columns, and sizes of systems, critical parameters, and critical exponents are in the rows. The last column gives the width of the window in which FSS was performed. The statistical errors referring to the last significant digits are indicated in parentheses.

	U_2	m	Δ	χ	$ \tilde{\lambda}L^{\frac{1}{\nu}} $
18 - 16					
λ_c	0.9857(28)	1.0050(7)	0.9998(3)	1.0062(2)	<2.0
ν	1.0051(20)	0.9186(47)	1.0123(20)	0.8945(53)	<2.0
β	—	0.1265(13)	—	—	<2.0
γ	—	—	—	1.7576(18)	<2.0
18 - 16 - 14					
λ_c	0.9835(19)	1.0051(7)	0.9992 (8)	1.0064(6)	<2.0
ν	1.0044(31)	0.9157(23)	1.0360(34)	0.8926(55)	<2.0
β	—	0.1253(15)	—	—	<2.0
γ	—	—	—	1.7529(33)	<2.0
14 - 10 - 6					
λ_c	0.9565(36)	1.0095(31)	0.9999 (10)	1.0226(18)	<1.0
ν	1.0150(47)	0.8680(43)	1.0843(64)	0.8149(75)	<1.0
β	—	0.1200(35)	—	—	<1.0
γ	—	—	—	1.6760(63)	<1.0
14 - 6					
λ_c	0.9587(49)	1.0126(45)	0.9998 (12)	1.0278(29)	<1.0
ν	1.0143(51)	0.8673(63)	1.0806(78)	0.8340(69)	<1.0
β	—	0.1236(27)	—	—	<1.0
γ	—	—	—	1.6135(61)	<1.0

TABLE II. Critical points and critical exponents obtained for TFIM on Sierpiński gasket lattice from finite-size scaling analysis of small systems. The quantities used for FSS are in the columns, and sizes of systems, critical parameters, and critical exponents are in the rows. The last column gives the width of the window in which FSS was performed. The statistical errors referring to the last significant digits are indicated in parentheses.

	U_2	m	Δ	χ	$\tilde{\lambda}L^{\frac{1}{\nu}}$
15 - 11					
λ_c	2.7239(18)	2.9304 (57)	2.7034 (40)	2.7801(58)	1.0
ν	1.1296(17)	1.0962(64)	1.1296(17) ^a	1.5544(89)	1.0
β	—	0.3002(45)	—	—	1.0
γ	—	—	—	2.5383(74)	1.0
z	—	—	0.8400(27)	—	1.0

^a To find z , we used ν obtained from scaling the Binder cumulant.

TABLE III. Critical coupling and β exponent obtained using the NRG method for 1D chain and the Sierpiński gasket.

1D chain	$N=2$	$N=3$	$N=4$	$N=5$
λ_c	1.276	1.154	1.106	1.080
β	0.393	0.182	0.191	0.162
Sierpiński gasket				
λ_c	2.984	2.765		
β	0.639	0.306		